Supporting Information

Exploring the Limits of the Rapid-Charging Performance of Graphite as the Anode in Lithium-Ion Batteries

Wei Xu[a], Connor Welty[a], Margaret R. Peterson[a],
Jeffrey A. Read[b], and Nicholas P. Stadie[a]*

[a]Department of Chemistry & Biochemistry, Montana State University, Bozeman, MT 59717, United States

[b]Battery Science Branch, Sensors and Electron Devices Directorate, Army Research Laboratory, Adelphi, MD 20783, United States

*Email: nstadie@montana.edu

Table of Contents:

S1. Three-Electrode Cell Schematic

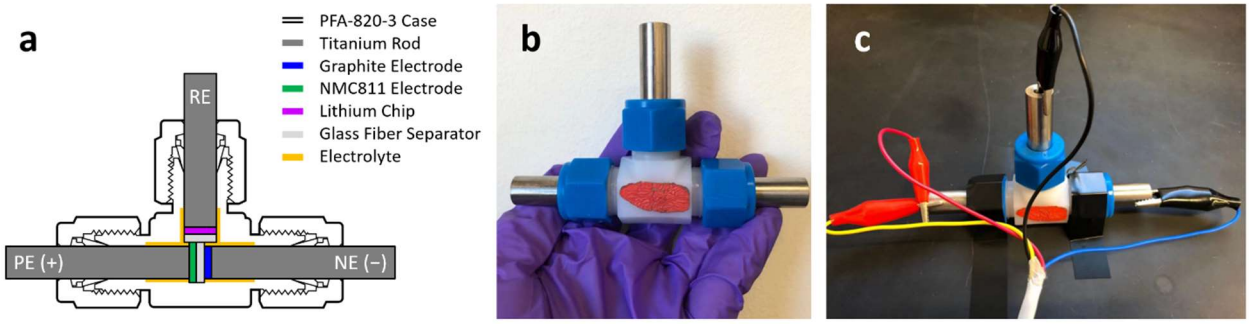

Figure S1. Three-electrode cell comprising graphite as the working electrode, NMC811 as the counter electrode, and lithium metal as the reference electrode. (a) Schematic diagram showing the internal view of the cell. Photographs of (b) the outer case and current collectors of a closed cell and (c) a cell during operation, showing the 4-point connection to the potentiostat.

S2. Surface Area Characterization

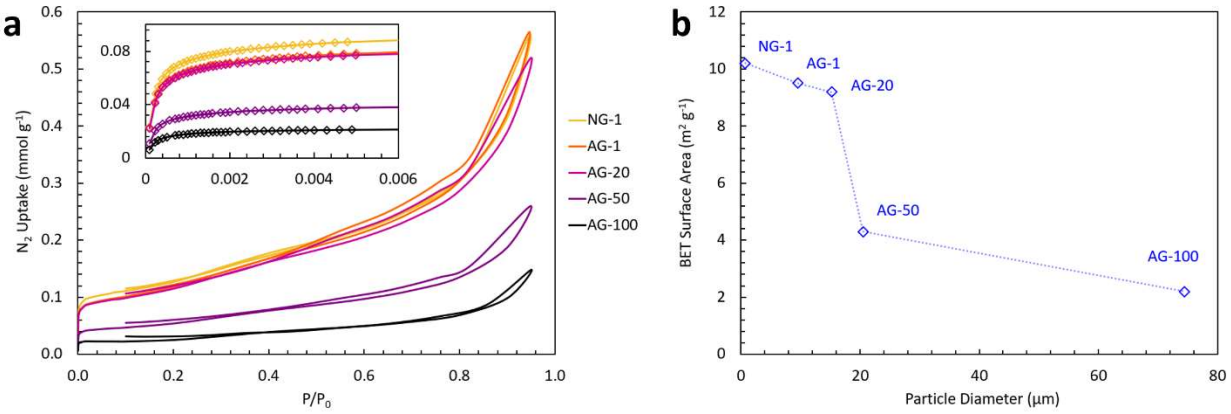

Figure S2. (a) Adsorption/desorption of N_2 at 77 K on five commercial graphite powders with nominal particle size of 1-100 μm: NG-1, AG-1, AG-20, AG-50, and AG-100, and (b) corresponding BET surface area as a function of actual particle size.

Table S1. Brunauer-Emmett-Teller (BET) N_2-accessible surface areas of the five graphite samples shown in **Figure S2**.

Graphite	BET Surface Area ($m^2\ g^{-1}$)
NG-1	10.2
AG-1	9.5
AG-20	9.2
AG-50	4.3
AG-100	2.2

S3. Further XRD Characterization of NG-1

The XRD pattern of NG-1 exhibits an excellent fit to the hexagonal unit cell of a graphite-like material with ABC stacking (ICDD database PDF# 00-26-1076), commonly described as a metastable form of nanocrystalline graphite, as shown in **Figure S3**.

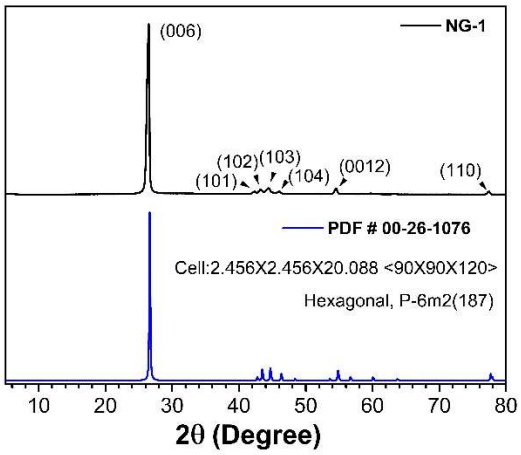

Figure S3. XRD patterns of (top) NG-1 and (bottom) a reference material (PDF# 00-26-1076).

S4. Further Raman Characterization

Raman spectra of the graphite samples explored in this work are shown in **Figure S4**. The full-width half-maximum of the G peak was used as the primary indicator of graphitic (in-plane) ordering. The position of the G peak as well as the I_D:I_G ratio, both often used in this context, are complexly related to crystallinity and should therefore not be used. The outlier in our analysis, as compared to XRD analysis, was NG-1, which showed a relatively narrow Raman G peak (**Figures 2e** and **S4a**) but a relatively broad XRD (002) reflection (**Figure 2b**). The ranking of NG-1 as an intermediate crystallinity sample is re-confirmed by intercomparison of the Raman 2D peak region of all five samples, showing features of nanocrystalline graphite for samples NG-1, AG-1, and AG-20 while showing features of highly crystalline graphite for AG-50 and AG-100.

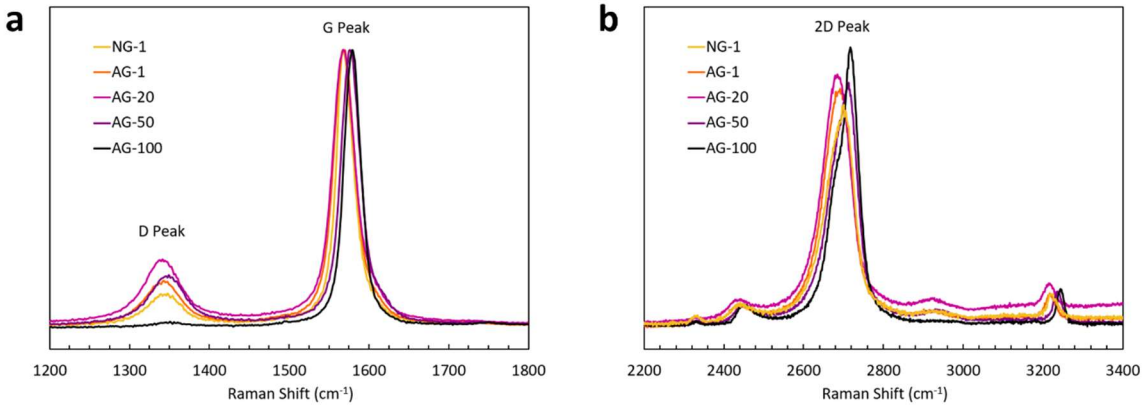

Figure S4. Raman spectra of the five commercial graphite powders with a nominal particle size of 1-100 µm: NG-1, AG-1, AG-20, AG-50, and AG-100: (a) around the D and G peaks and (b) around the 2D peak.

S5. Lithium Plating Onset Determination

The five different sized graphites explored herein (with nominal particle size: ~0.4-1.2, ~1, 20, 50, and 100 µm) were prepared as anodes with a narrow range of loadings from 2.4-2.7 mg cm^{-2}, and mated with a standard NMC811 cathode (of loading 9.08 mg cm^{-2}); 2032-type coin cells were assembled in an Ar-filled glovebox. Charging was performed at 50 mA g^{-1} for 3 replicate cells of each graphite size. All cells displayed a similar voltage increase and recovery feature ("voltage delay") around 490-500 mAh g^{-1}, followed by a long plateau, as shown in **Figure S5**. This plateau is indicative of the onset of Li plating on the graphite electrode. These results show that the graphite potential is reduced to below 0 V vs. Li/Li^+ at ~500 mAh g^{-1}. The voltage delay effect has generally been attributed to differences in the solid-electrolyte interface or the formation of a passivation layer on the anode surface during initial stages of reduction. Thus, the voltage delay phenomenon in the first charging profile is attributable to a thin layer of lithium metal formed at the onset of the plating process, followed by further Li deposition on that layer.

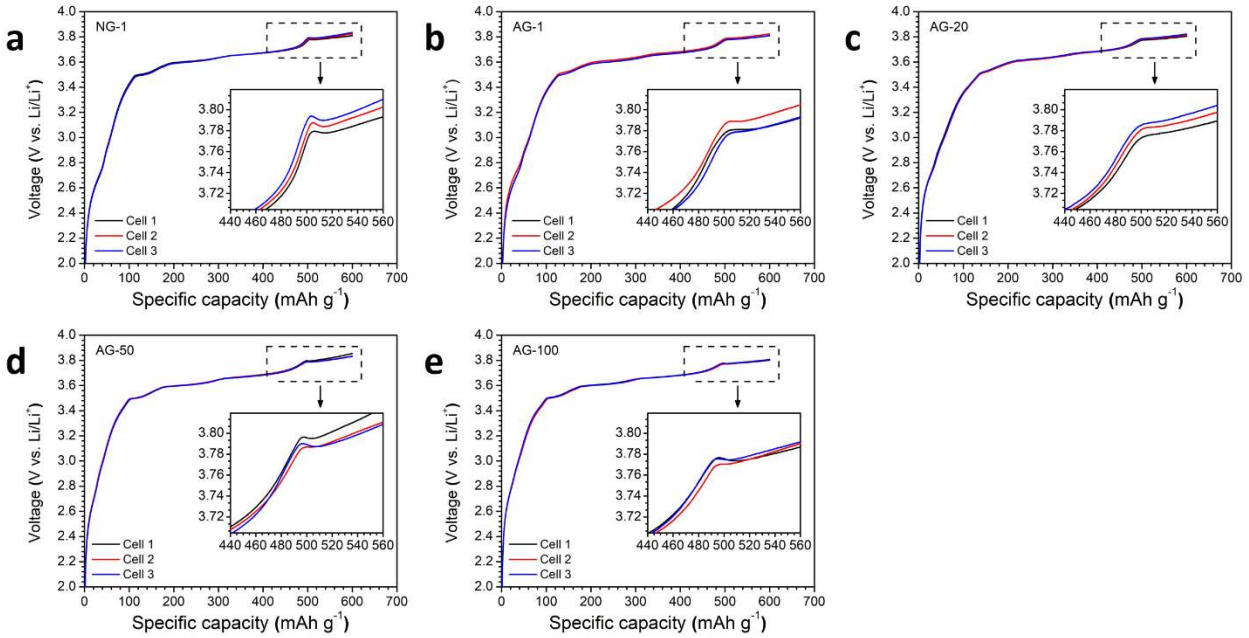

Figure S5. Voltage profiles during the first charge of each type of graphite within three-electrode full-cells containing NMC811 as the cathode, Li metal as the reference electrode, and (a) NG-1, (b) AG-1, (c) AG-20, (d) AG-50, or (e) AG-100 as the anode.

S6. Preliminary Results of N:P Ratio Investigations

The electrochemical performance of six different anode-limited full-cells using 1.46, 1.27, and 1.09 mAh cm^{-2} as the graphite loadings coupled with a fixed 1.50 mAh cm^{-2} NMC811 positive electrode are shown in **Figure S6**. This corresponds to N:P ratios of N/P = 0.97, 0.85, and 0.73; each N:P ratio was explored in duplicate. The higher anode loadings (1.46 and 1.27 mAh cm^{-2}) displayed significant capacity decay in the 0.2 C rest cycles, especially for the 1.46 mAh cm^{-2} cells, and obvious capacity fading at the fast-rate cycling. Improvement was observed for N/P = 0.73 (1.09/1.50 mAh cm^{-2}) with relatively stable cycling at faster rates and only a slight capacity fading within the 0.2 C rest cycles at ≥4 C. Therefore, only low N:P ratios below N/P = 0.73 were selected for further investigation in this work (as shown in **Figure 4**).

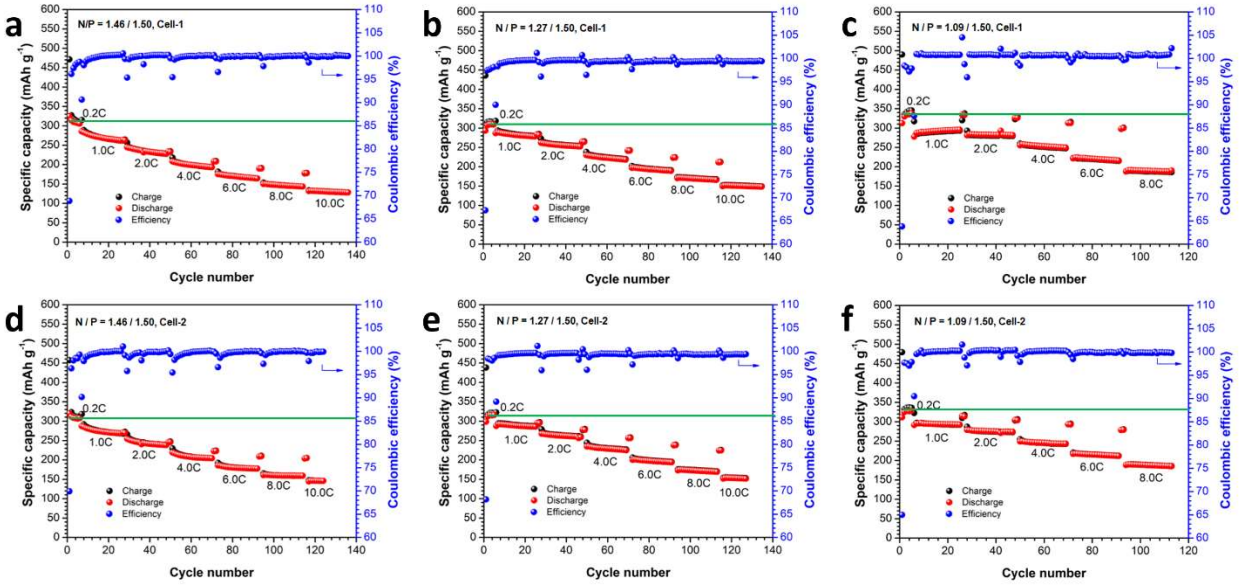

Figure S6. Preliminary N:P ratio optimization using AG-20 as the anode, NMC811 as the cathode, and a two-electrode coin-cell configuration, under a rate capability test with 0.2 C rest cycles between high-rate intervals. Three N:P ratios were explored: (a,d) N/P = 0.97, (b,e) N/P = 0.85, and (c,f) N/P = 0.73. The areal capacities of each electrode are indicated.

S7. Additional Electrochemical Characterization

To compare the rapid-charging performance of the five different commercially-available graphite powders explored in this work, the rate capability was characterized under identical conditions within full-cells consisting of graphite as the anode, NMC811 as the cathode, and an EC/EMC-based electrolyte, with an N:P ratio of N/P = 0.67. These cells were tested at current rates of 4-20 C, employing a CCCV charging protocol followed by a 1 C CC discharging protocol, with three 0.2 C charging cycles inserted between each interval. Five replicate cells were averaged for each different graphite powder to produce the results shown in **Figures 5a-5b** and **Figures S7-S8**.

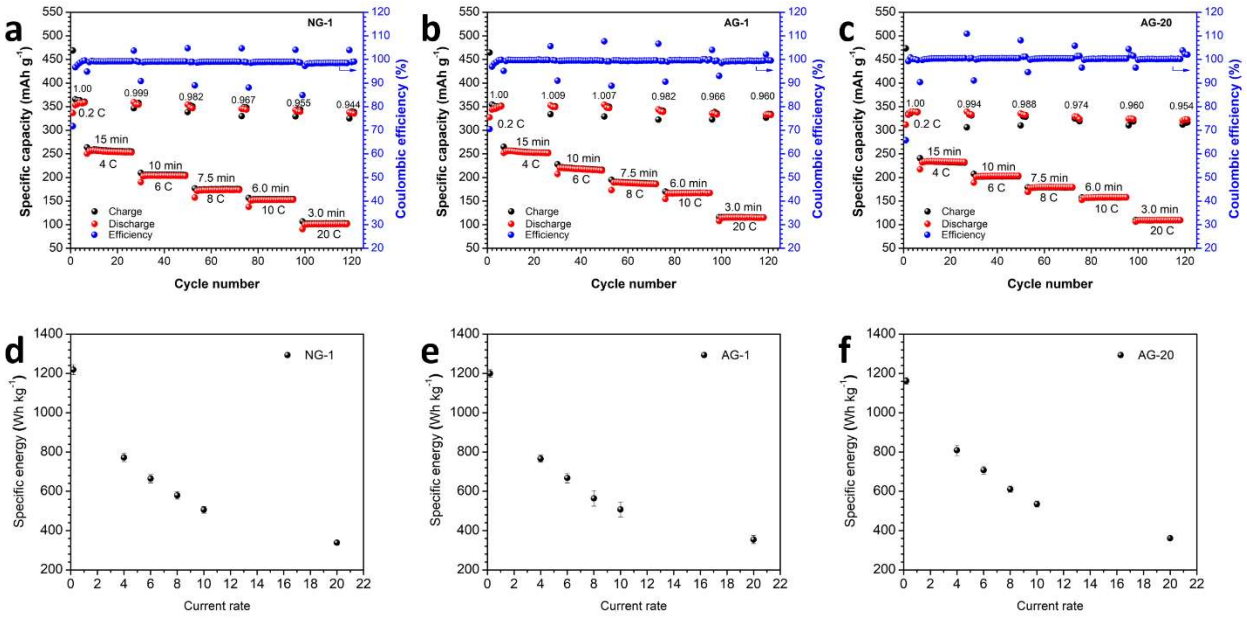

Figure S7. (a-c) Charge/discharge capacity (red/black, respectively) and coulombic efficiency (blue) as a function of cycling for full-cells with N/P = 0.67 at increasing current rates up to 20 C. (d-f) Reversible specific energy (20th cycle) as a function of current rate. Three graphites are shown: (a,d) NG-1, (b,e) AG-1, and (c,f) AG-20.

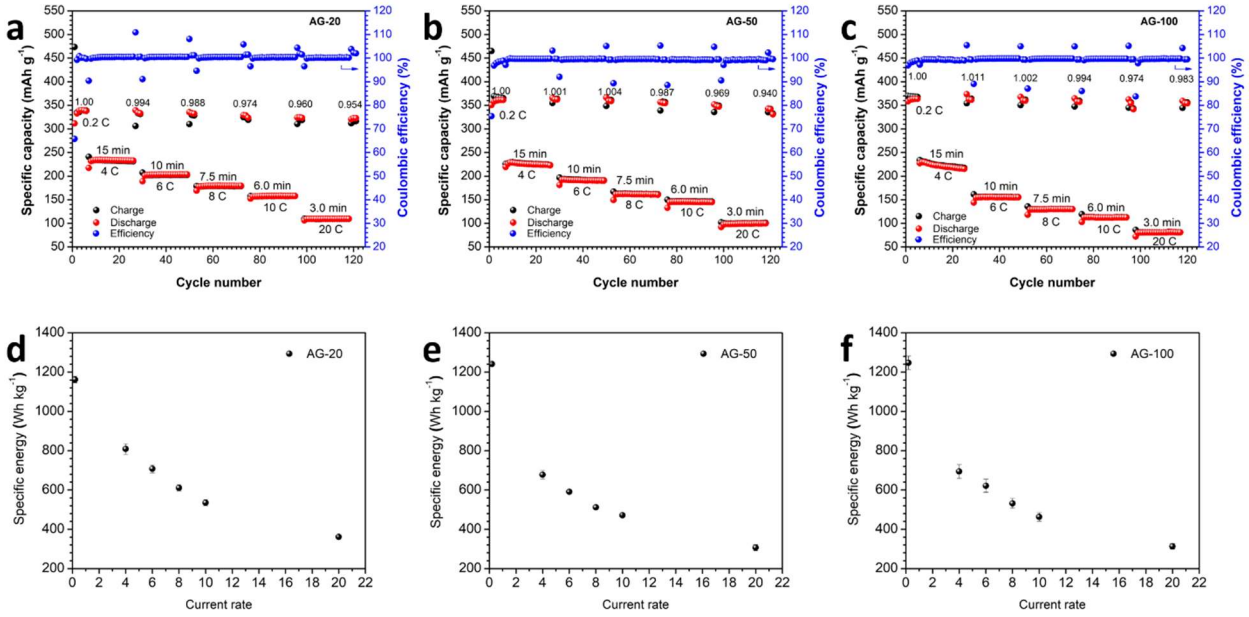

Figure S8. (a-c) Charge/discharge capacity (red/black, respectively) and coulombic efficiency (blue) as a function of cycling for full-cells with N/P = 0.67 at increasing current rates up to 20 C. (d-f) Reversible specific energy (20th cycle) as a function of current rate. Three graphites are shown: (a,d) AG-20, (b,e) AG-50, and (c,f) AG-100.

S8. High-Precision Coulometry

High-precision coulometry (HPC) can be used to sensitively detect the onset of lithium plating within a two-electrode cell (as established elsewhere[38-40]). This approach is founded on the principle that the coulombic efficiency of a cell will decrease slightly when lithium plating occurs; since this is a subtle effect, a high-precision measurement of the efficiency is required, typically also requiring precise control and measurement of the temperature of the cell. When inverted and normalized per unit time, this effect can also be quantified as coulombic inefficiency per hour (CIE h^{-1}); a positive CIE is attributable to lithium plating. As the rate increases, the CIE h^{-1} becomes even more sensitive to lithium plating; therefore, if plating begins at a particular current rate during a rate capability test comprising intervals of increasing current rate, the CIE h^{-1} is expected to significantly increase. No obvious increase in CIE h^{-1} is observed in any of the cells investigated herein, as shown in the representative cases presented in **Figures S9-S10**. All measurements were performed using a Novonix RCA-CCC-12-00 18U high-precision coulometry system containing an 8 channel module (CMA-HDX-99-56, 2A) and a standard thermal chamber (TCA-WLS-12-60).

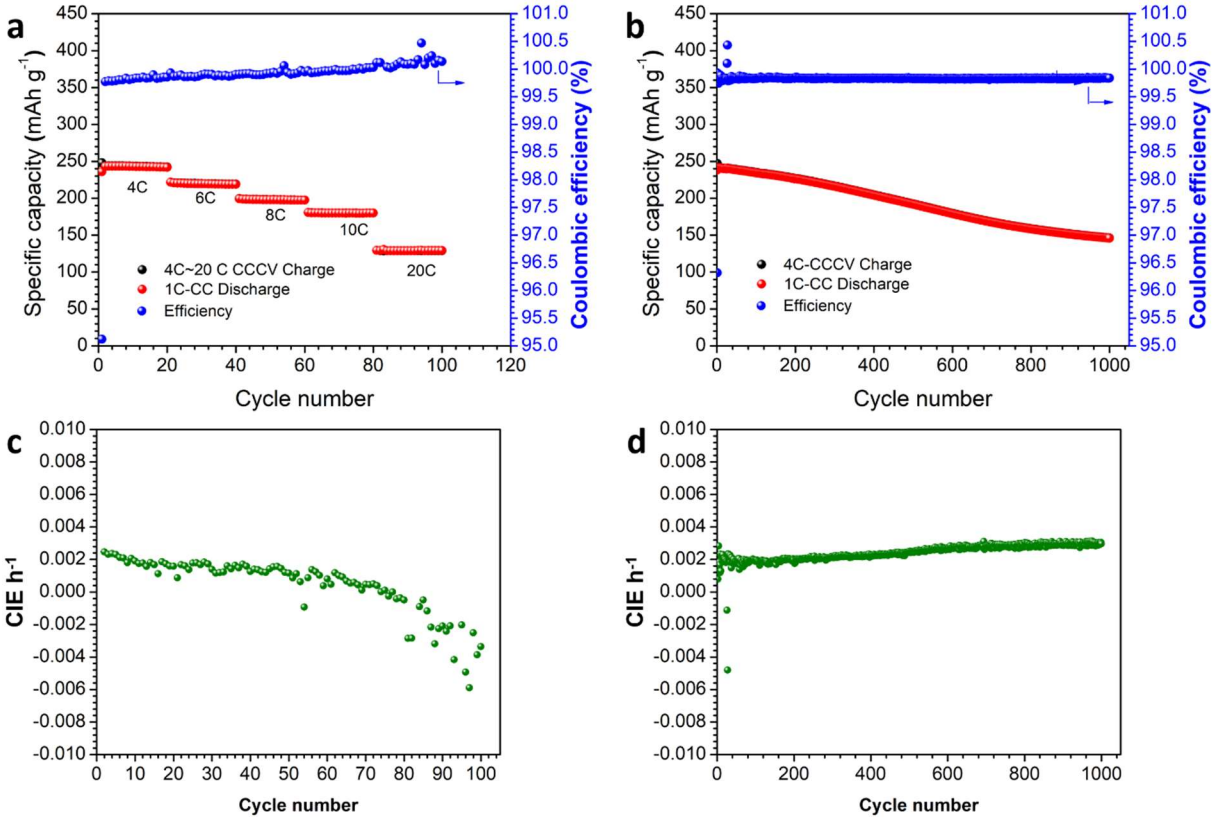

Figure S9. High-precision coulometry (HPC) studies of two-electrode full-cells comprising AG-20 as the anode (1.0 mAh cm^{-2}) and NMC811 as the cathode (1.5 mAh cm^{-2}) at current rates from 4-20 C using CCCV charging and a universal 1 C CC discharge. (a,c) Rate capability test comprising 20 cycle intervals at increasing current rates from 4-20 C and (b,d) long-term cycling at a current rate of 4C.

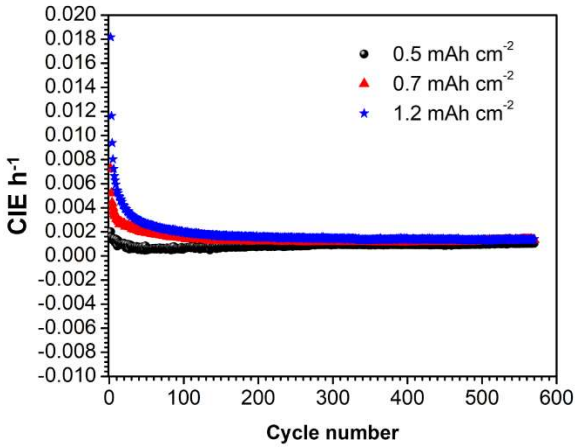

Figure S10. High-precision coulometry studies of two-electrode full-cells comprising AG-20 as the anode (at varying loadings as indicated) and NMC811 as the cathode at a current rate of 4 C using CCCV charging and a universal 1 C CC discharge. The anode loadings were 0.5 (black), 0.7 (red), and 1.2 (blue) mAh cm^{-2}, coupled with an appropriate cathode loading to maintain N/P = 0.67.

HPC References

[38] T. M. Bond, J. C. Burns, D. A. Stevens, H. M. Dahn, and J. R. Dahn, *J. Electrochem. Soc.*, 160, A521 (2013).

[39] J. C. Burns, D. A. Stevens, and J. R. Dahn, *J. Electrochem. Soc.*, 162, A959 (2015).

[40] J. E. Harlow, S. L. Glazier, J. Li, and J. R. Dahn, *J. Electrochem. Soc.*, 165, A3595 (2018).

S9. Energy and Power Calculations

As a representative example, we demonstrate the calculations of specific energy and specific power based on a summary of the results for AG-20 at a current rate of 4 C. These data are then used to obtain a Ragone plot of charged power as a function of discharged energy (**Figure 6d**). All data were measured at 25 °C.

First, the specific capacity of a full-cell (containing NMC811 as the cathode) was measured as a function of active mass of graphite within the anode. Representative results for one such cell are shown in **Figure 5a**. Five such cells were averaged in order to ensure statistical reliability. The 20th cycle capacity under a given current rate was used as the final capacity for a given cell.

For AG-20 at 4 C, the average discharge capacity, Q, was found to be 230.5 mAh g^{-1} (normalized per mass of AG-20). The average discharge voltage was determined by integration of the voltage profile of the same cycle for each cell; over all five cells, the average discharge voltage, V_{avg}, was found to be 3.509 V.

The specific energy was then calculated as:

$$E = Q \cdot V_{avg}$$

The specific discharged energy at 4 C was found to be 808.8 Wh kg^{-1} (still normalized per mass of AG-20).

The specific power was then calculated based on the charging time, t, as:

$$P = \frac{E}{t}$$

The specific power upon charging at 4 C was thus found to be 3235 W kg^{-1} (still normalized per mass of AG-20) based on an exact charging time of 15 min for a 4 C CCCV charging protocol.

To estimate the "true" specific energy, E_{fc}, and power, P_{fc}, of an entire full-cell, the fraction of the mass of the cell that is attributed to the active graphite, α, must be known. Then:

$$E_{fc} = \alpha \cdot E$$

$$P_{fc} = \alpha \cdot P$$

To estimate α, toward modeling the performance of battery cells developed for electric vehicles, a software package called BatPaC has been provided by Argonne National Laboratory (ANL) to determine the actual mass of a full-cell containing a specific cell chemistry and N:P ratio, and designed for a specific end use. The full-cell mass includes electrodes (active material, additives,

and binder for each), electrolyte (amount specified depending on cell design), separators, current collectors, and all other components to build a working cell, including a PET-Al-PP cell container. Two scaling factors, α_1 and α_2, were determined in this work: α_1 = 0.2616 for a plug-in hybrid electric vehicle (PHEV) and α_2 = 0.3320 for a micro-hybrid electric vehicle (m-HEV). These were selected as representing the worst- and best-case scenarios provided within the BatPaC software, respectively.

The range of specific energy and power for an AG-20-based full-cell (N/P = 0.67) at 4 C are thus determined to be:

$$E_{fc,1} = \alpha_1 \cdot E = 211.6 \text{ Wh kg}^{-1}$$

$$P_{fc,1} = \alpha_1 \cdot P = 846.3 \text{ W kg}^{-1}$$

$$E_{fc,2} = \alpha_2 \cdot E = 268.5 \text{ Wh kg}^{-1}$$

$$P_{fc,2} = \alpha_2 \cdot P = 1074 \text{ W kg}^{-1}$$

More information about BatPaC can be found here:
https://www.anl.gov/tcp/batpac-battery-manufacturing-cost-estimation